LBM, a Useful Tool for Mesoscale Modelling of Single Phase and Multiphase Flow – the variety of applications and approaches at Nottingham

Yuying YAN*, Yingqing ZU, Bo DONG

* Corresponding author: Tel.: ++44 (0)115 951 3169; Fax: ++44 (0)115 951 3159;
Email: yuying.yan@nottingham.ac.uk
School of the Built Environment, University of Nottingham, UK

Abstract Giving an overview of Nottingham group's recent progress on numerical modelling and approaches in developing and applying the lattice Boltzmann method (LBM), the paper tries to demonstrate that the LBM is a useful tool for mesoscale modelling of single phase and multiphase flow. The variety of applications of the LBM modelling is reported, which include single phase fluid flow and heat transfer around or across rotational cylinder of curved boundary, two-phase flow in mixing layer, electroosmotically driven flow in thin liquid layer, bubbles/drops flow and coalescence in conventional channels and in microchannels with confined boundary, liquid droplets in gas with relative large density ratio; viscous fingering phenomena of immiscible fluids displacement, and flow in porous media.

Keywords: LBM, multiphase flow, mixing layer, electroosmosis flow, drops, bubbles, coalescence, wetting, hydrophobic, large density ratio

1. Introduction

In recent years, along with extensive applications of conventional computational fluids dynamics (CFD) to the study of fluids flow and transport phenomena, the lattice Boltzmann method (LBM) has become an established numerical scheme for simulating single phase and multiphase fluid flows. The key idea behind the LBM is to recover correct macroscopic motion of fluids by incorporating the complicated physics of problems into simplified microscopic models or mesoscale kinetic equations. In this method, kinetic equations of particle velocity distribution functions are first solved; macroscopic quantities are then obtained by evaluating hydrodynamic moments of the distribution function. This intrinsic feature enables the LBM to model phase segregation and interfacial dynamics of multiphase flow, which are difficult to handle by conventional CFD or the molecular dynamics (MD) method. Since the foundation of the first lattice Boltzmann model for multiphase flow in 1991, a number of multiphase and multi-component models based on LBM have been introduced (Succi, 2001). To date, the LBM has demonstrated a significant potential and broad applicability with many computational advantages including the easy parallelisation and the simplicity of programming (Chen & Doolen, 1998). Based on the two-component lattice gas method, Gunstensen et al. (1991) proposed a multi-component model; Shan & Chen (1993) have initiated a pseudo-potential model which has the capacity of simulating multiphase and multi component immiscible fluid flow of mean-field interactions, and the model was later analysed and evaluated carefully in Shan et al., 1994, 1995, 1996, and Martys et al., 2001). Meanwhile, Swift et al. (1995, 1996) proposed the free energy model, in which the Van der Waals formulation of quasi-local thermodynamics for two component fluid in thermodynamic equilibrium state is built. Later, a new LBM model called index model was suggested by He et al. (1999) which use index function to track the interface of multi-phase flow with large density ratios. To overcome the difficulties of dealing with large density ratio of two-phase flow, Inamuro et al. (2004) developed a LBM model based on the projection method to predict the behaviours of incompressible bubbles/particles in bulk liquid.

The method calculates two distribution functions of particle velocity to track the interface and to predict velocities; the corrected velocity field satisfying the continuity equation is obtained by solving the Poisson equation. On the above basis, Yan & Zu (2007a) developed the LBM model for incompressible two-phase (with large density ratio) flow on a partial wetting surface and the method is applied to the present simulation.

A variety of applications of LBM modelling has been attempted by the authors at Nottingham since 2006; these are summarised and reported in the following sections.

2. Fluid Flow and Heat Transfer across Rotational Cylinders of Curved Boundary

Fluid flow around a rotating isothermal cylinder (or between two rotating cylinders) is a common occurrence in a variety of industrial processes, such as contact cylinder dryers in the chemical process, food-processing, paper making and the textile industries to the cylindrical cooling devices in the glass and plastics industries. Although this is a single-phase flow problem as shown in Fig. 1, the LBM modeling of such flow is concerned with effective treatment of moving and curved boundaries, and considering heat transfer. In the numerical approach, a D2Q9 LBM model with multiple distribution functions was employed to simulate incompressible viscous thermal flow (Yan & Zu, 2008a).
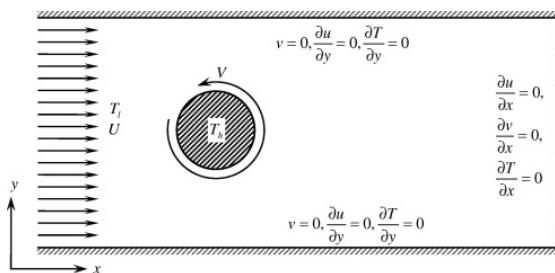

Fig. 1: flow field set-up

An extrapolation method for dealing with the curved boundaries of temperature and velocity fields was developed based on Guo, et al., 2002; Mei, et al, 2002) and can achieve second-order accuracy for both velocity and temperature on the curved wall.

The modelling was well validated against experiment. Useful results were obtained, such as Fig. 2 shows the distributions of local Nu number at Re=200, Pr=0.5, $\theta \in [-\pi/2, \pi/2]$ for ratio of rotational velocity and inflow velocity at k=0.0, 0.1 and 0.5, respectively.
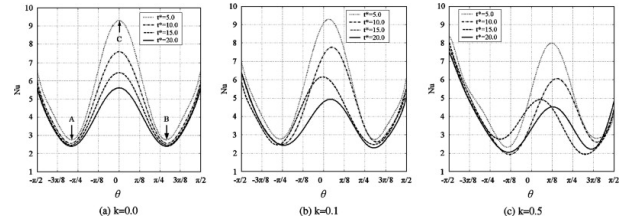

Fig. 2: Distributions of local Nusselt numbers for Re=200, Pr=0.5, $\theta \in [-\pi/2, \pi/2]$.

3. Two-phase Flow in Mixing Layer

Mixing layers can often be observed in flow fields of many engineering applications such as in combustion chambers, pre-mixers of gas turbine combustors, chemical lasers, propulsion systems, flow reactors, micro mixers, etc. Controlling the formation and evolution of the coherent structure in a mixing layer can normally improve efficiencies of combustion, chemical reaction, etc. Certain flow features of mixing layers such as the instability of flow, evolutions and interactions of vortices layers have drawn attentions of both experimental and computational studies.

The index model (He, et al., 1999) was employed to study vortices merging in a two-dimensional (based on D2Q9) two-phase spatial growing mixing layer (Yan and Zu, 2006). With an initial velocity field which consists of a hyperbolic tangent profile as defined in Fig. 3, phase distributions of three vortices merging with values of different surface tension were obtained.
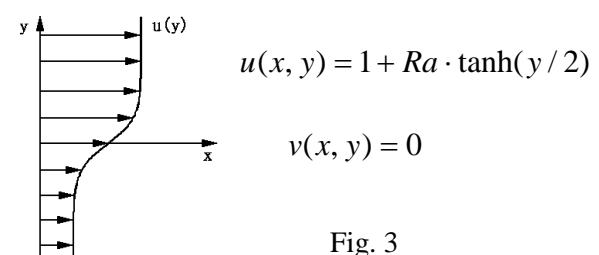

$$u(x, y) = 1 + Ra \cdot \tanh(y/2)$$

$$v(x, y) = 0$$

Fig. 3

Fig. 4 shows the phase distribution of zero surface tension compared with one of surface tension coefficient at k=0.1. Fig. 5 shows

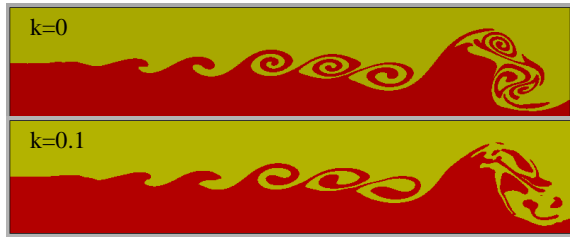interface distributions and the corresponding vortices contours with different values of surface tension.

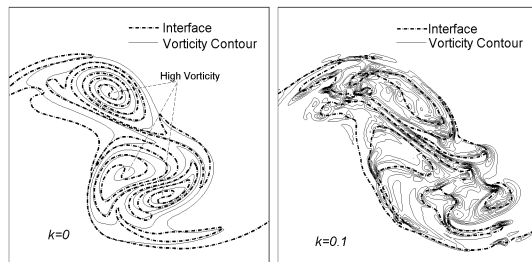Fig. 4: Phase distribution of three vortices merging

Fig. 5: the interface distribution

4. Electroosmotically Driven Flow in Thin Liquid Layer

The electro-osmotic flow near an earthworm body surface is a basic electrokinetic phenomenon that takes place when the earthworm moves in moist soil. The flow within a micro thin liquid layer near the earthworm's body surface is induced by the electric double layer (EDL) interaction. The modelling (Zu & Yan, 2006; Yan, et al, 2007) incorporated the lattice Poisson method (LPM) for electric potential in the EDL and the LBM (D2Q9 and index model (He et al. 1999)) for fluid flow with external electric body force. Fig. 6 shows streamline evolution of electro-osmotically driven flow within the thin liquid layer near an earthworm body surface. The moving vortices shown may play a major role in anti- soil adhesion.
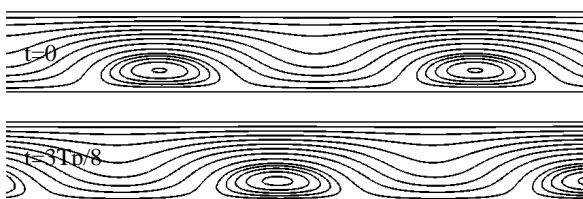

Fig. 6: Stream evolution near earthworm surface

5. Modelling of Viscous Fingering Phenomena of Immiscible Displacement

5.1 The displacement in a channel

The wettability of reservoir rocks plays an important role in oil recovery industry, which is recognised to be capable of affecting the properties of fluid-rock interactions, such as residual oil saturation, relative permeability and capillary pressure. Practically, wettability alternation can be achieved by injecting surfactants, altering salinity, and increasing temperature. In the oil industry, when supercritical carbon dioxide (SCO_2) is injected into a reservoir, the wettability of reservoir rocks can be changed due to a series of reaction of SCO_2, crude oil and rock materials. In the LBM modelling, we focus on the effect of wettability of rocks on viscous fingering phenomenon which can account for the breakthrough of the displacing fluid. Additionally, the effect of gravity is considered, even at the pore scale level, still has an impact on fluid distribution and its patterns.

A pseudo-potential D2Q9 model (Shan & Chen, 1993) was employed to the modelling. In addition, the formulation of fluid-solid interaction (Martys and Chen, 1996) was considered and applied. The effects of Capillary number, Bond number, viscosity ratio and the channel surface wettability on the fingering phenomenon are evaluated through a series of numerical simulations.

Fig. 7 shows the effect of gravity on the offsets of finger width and finger length under different conditions of wettability in terms of the strength of fluid-solid interaction Gw1 (Dong, et al., 2009).
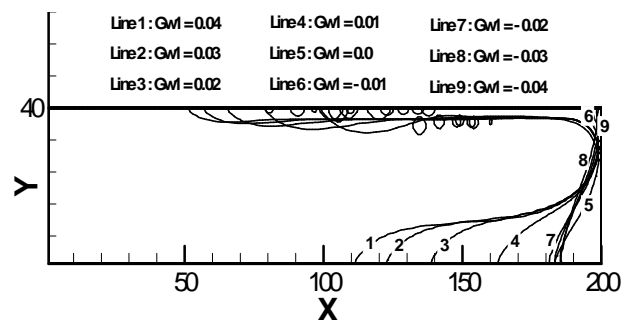

Fig. 7: the effect of gravity on finger patterns

5.2 The displacement in porous media

The pseudo-potential LBM D2Q9 model (Shan & Chen, 1993) was employed for the modelling. The effect of capillary number, Bond number and the viscosity ratio of two immiscible fluids on viscous fingering phenomena were simulated and discussed. Fig. 8 shows the interface positions at final stage of the displacement process with different Bond numbers; the interface front has a tendency to move downwards under the action of gravity.
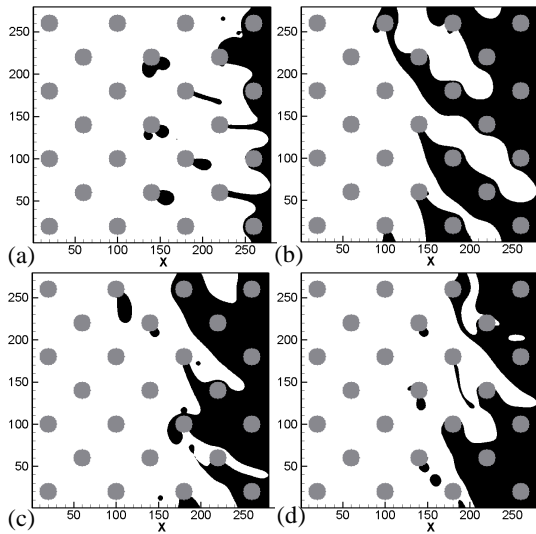

Fig. 8: Final finger patterns (a) $Bo = 2.79$; (b) $Bo = 5.58$; (c) $Bo = 8.37$; (d) $Bo = 11.16$.

6. LBM Modelling of Bubbles and Droplet on Wetting Surface

A major work of LBM modelling at Nottingham aiming to improve the suitability of LBM for simulating two-phase fluids flow of large ratios of densities and viscosities was presented (Yan & Zu, 2007). In addition to deal with large density ratio or viscosity ratio, the LBM model can also deal with fluids interaction with solid surface of different wettability or hydrophobicity (Yan, 2009); this makes the LBM to be more attractive tool for simulating two-phase flow problems in engineering and industrial processes.

A D3Q15 free energy lattice Boltzmann method is used for three-dimensional modeling. To simulate flows with large density and/or viscosity ratio, a projection method (Inamuro et al., 2004) is employed. In the method, two particle velocity distribution functions are used. One is for calculating the order parameter; the other is for calculating the predicted velocity field without pressure gradient. The corrected velocity satisfying the continuity equation can be obtained by solving a Poisson equation.

In order to realize the partial wetting on solid surfaces to agree with the Cahn theory (Cahn, 1977), a wetting boundary condition is introduced. According to Young's law, when a liquid-gas interface meets a partial wetting solid wall, the contact angle, θ_w, measured in the liquid, can be calculated from a balance of surface tension forces at the contact line as

$$\cos\theta_w = \frac{(1+\Omega)^{3/2} - (1-\Omega)^{3/2}}{2}$$

where Ω is the wetting potential and can be represented by surface tensions σ_{SG}, σ_{SL} and σ_{LG} (Yan and Zu, 2007). To calculate such surface tensions within a mean field framework, Cahn (1977) assumed that the fluid-solid interactions are sufficiently short-range so that they contribute a surface integral to the total free energy of the system. To calculate wall-fluid surface tensions in a closed form, a new form of free energy (rather than the van der Waals free energy used in the traditional free energy model) is used (Yan & Zu, 2007). Based on such method reported, the motions of bubble and droplet with the effects of confined boundary are simulated. The ratio of densities of two fluids are from 775 to 1000 (for water to air), and the ratio of dynamic viscosities is of 50. The initial surface tension between water and air is of $\sigma_{LG} = 1 \times 10^{-3} kg/s^2$ and the gravitational acceleration is set at $g = 9.8 m/s^2$.

6.1 Bubbles flow and coalescence

The modelling is concerned with the motion of air bubbles surrounded by water flow in a horizontal rectangular microchannel (Yan & Zu, 2008b). Initially, two air bubbles with same diameter $d = 200\mu m$ are placed $300\mu m$ apart in water inside a rectangular channel of the length $L_x = 1200\mu m$, the width and the height $L_y = L_z = 300\mu m$. The channel

has an inlet boundary on the left hand side of the channel and a free outflow boundary on the right hand side of the channel. The other four sides of the channel are no-slip solid walls.

The velocity distribution at the inlet boundary is specified as,

$$\begin{cases} u_x(0, y, z) = 16U(L_y - y)(L_z - z)yz/(L_yL_z)^2; \\ u_y(0, y, z) = 0; \\ u_z(0, y, z) = 0; \end{cases}$$

where, U is the maximum value of $u_x(0, y, z)$.

The bubbles flow in the microchannel at Reynolds number ($Re = \rho_L UL_x / \mu_L$) of 100 and Capillary numbers ($Ca = \mu_L U / \sigma_{LG}$) of 0.33 is simulated. The evolution with time of bubbles shapes and interaction are shown in Fig. 9. It can be seen clearly that the bubbles move in *x*-direction by the thrust force of surrounding water flow and meanwhile go up in *y*-direction due to the effect of buoyancy force; and with time marching, the two bubbles can finally coalesce into a larger one. To focus only on the shape evolution of the left bubble at the early stage, it is found that the lower part of the bubble moves more quickly in *x*-direction than the upper part, which is mainly caused by the effects of velocity boundary layer near the solid wall of the channel.
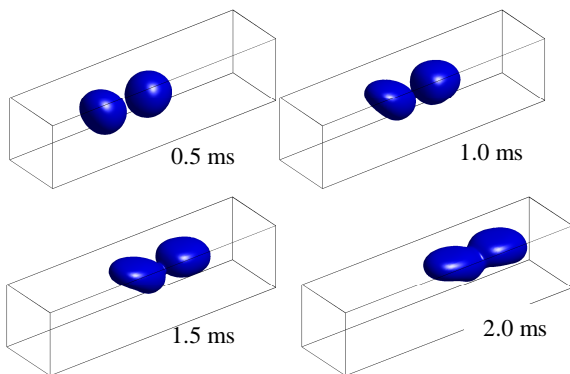

Fig.9: Evolution of bubble shapes

The velocity fields are obtained through the numerical modelling. For example, at t = 2ms, the velocity distribution at different cross sections of *y-z* plane such as $x = L_x / 2$, $2L_x/3$ and $3L_x/4$, respectively, is shown in Fig. 10; where the solid line, the constant density line,
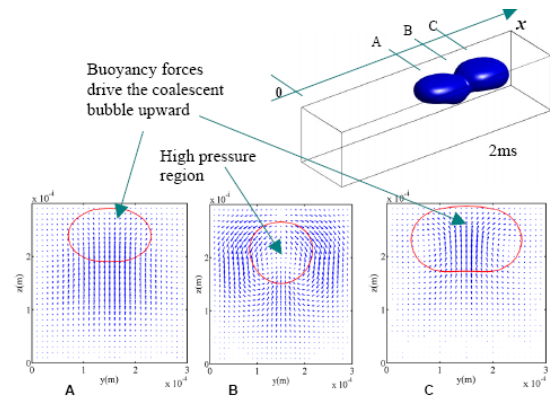
indicates the interface between the two phases.

Fig.10: Velocity field at cross section, t = 2ms, Re=100: (A: $x=L_x/2$, B: $x=2L_x/3$, C:$x=3L_x/4$).

Figs. 11(a) and (b) show the velocity vector and the vortices contours, respectively, at t= 2 ms, and at $y = L_y / 2$ on *x-z* plane. It can be seen that the local distribution in coherent structures is evident; the shape of the coalescent bubbles is a result of the interaction between the fields of velocity and density concentration, and this is mainly affected by the effects of buoyancy force of the bubbles (Mazzitelli, et al., 2003).
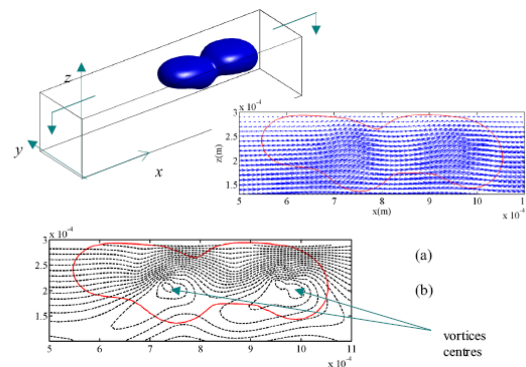

Fig. 11: Velocity vector and vortices contours of coalescent bubble at y = L_y / 2 on x-z plane for t = 2ms at Re = 100.

As both pressure and velocity distributions across the interface are normally excellent indicators of numerical stability for the LBM calculations (Lee and Lin, 2005), Figs. 10 and 11 have actually shown that the present LBM can be used to obtain reasonable and stable velocity fields. Indeed, similar to the conventional CFD, the numerical instabilities of the LBM for two-phase flow of large

density ratios are mainly caused by spurious velocities and/or the large oscillation of the pressure distribution across the phase interface. However, in the present method, the velocity and pressure are both corrected by solving an additional Poisson equation after each collision-stream step. Such corrections are able to ensure the velocity to satisfy the continuity equation and smooth pressure distributions even across the interface, so that to ensure the numerical stability.

6.2 Droplet spreading on partial wetting surface

Water droplets in air spreading on a partial wetting wall are simulated (Yan & Zu, 2007). Fig. 12 shows how a small hemispherical water droplet evolves with time on a heterogeneous surface. A narrow hydrophobic strip with width of $l = 6 \times 10^{-4} m$ is located at the centreline of the surface where $\theta_w = 5\pi/6$, and the other areas are occupied by the hydrophilic surface with $\theta_w = \pi/6$. The initial droplet which has a radius $r = 1.5 \times 10^{-3} m$ is set at the centre of the wetting surface. As shown in the figure, the droplet stretches over the area occupied by the hydrophilic surface in the early stages of flow evolution due to the adhesive force of the surface. At the same time, the droplet rapidly contracts inward along the hydrophobic strip. With the development of time, the droplet spreads further on the hydrophilic area, and meanwhile contracts inward along the hydrophobic strip and finally breaks up into two smaller droplets. The newly formed droplets continue spreading until an equilibrium state is reached.

Then, a single droplet spreading on a heterogeneous surface with intersecting hydrophobic strips is simulated. As shown in Fig. 13, two cross hydrophobic strips ($\theta_w = 5\pi/9$) with width of $l = 9 \times 10^{-4} m$ are located at the centreline of the square surface, the other areas are occupied by the hydrophilic surface with $\theta_w = \pi/4$. Initially, the droplet has a shape of spherical cap with radius of $r = 2 \times 10^{-3} m$ and height of $h = 1 \times 10^{-3} m$,

and is set at the centre of the surface. The shape evolution of the droplet with time is shown in Fig. 13. From the figure, it can be seen that the droplet symmetrically spreads into four hydrophilic sections with the development of time and finally reaches an equilibrium state with a shape of four-leaved flower.
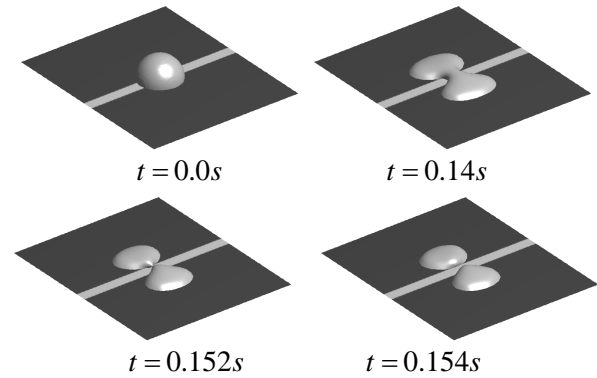

$t = 0.0s$ $t = 0.14s$

$t = 0.152s$ $t = 0.154s$

Fig. 12: Snapshots of a droplet spreading on a surface with a hydrophobic strip.
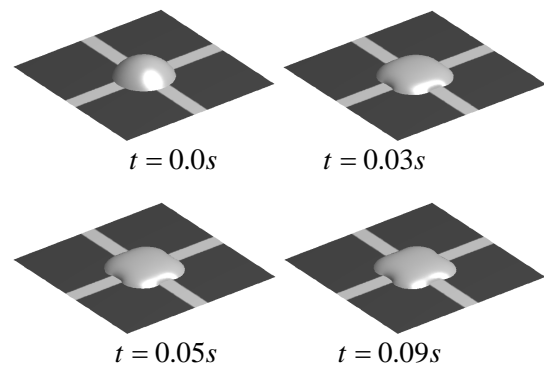

$t = 0.0s$ $t = 0.03s$

$t = 0.05s$ $t = 0.09s$

Fig. 13: Snapshots of a droplet spreading on a surface with intersecting hydrophobic strips.

Finally, the evolution of a water droplet spreading on the heterogeneous surface consisting of alternating and parallel hydrophilic strips with the width and the steady-state contact angle of $l = 7 \times 10^{-4} m$, $\theta_w = 2\pi/9$ and the hydrophobic strips with $l = 5 \times 10^{-4} m$ and $\theta_w = 5\pi/9$ is considered. Initially, the droplet has a shape of spherical cap with radius $r = 2 \times 10^{-3} m$ and height $h = 1 \times 10^{-3} m$; the centre of initial circular contact line is set on the hydrophilic surface and the minimum distances form it to two neighbouring hydrophobic strips are

$2 \times 10^{-4} m$ and $5 \times 10^{-4} m$ respectively. The behaviour of 3D droplet and the time evolution of the contact are shown in Figs. 14 and 15 respectively. It can be noted from the figures that, the droplet can finally reach a symmetric shape although the centre of the droplet is initially set at a location other than the centreline of any strip.

$t = 0.0s$ $t = 0.04s$
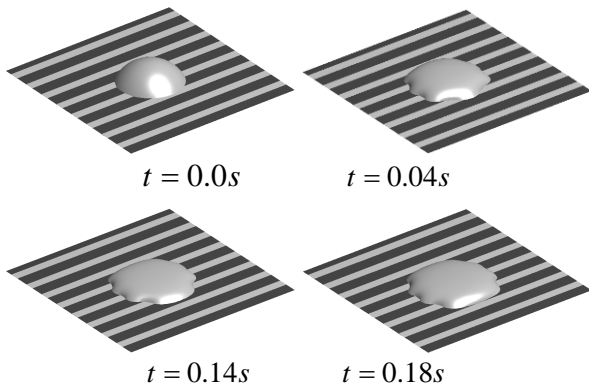
$t = 0.14s$ $t = 0.18s$

Fig. 14: Droplet spreading on a surface consisting of alternating and parallel strips.
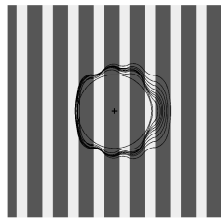

Fig. 15: Evolution of moving contact line on a surface with alternating and parallel strips.

As shown in Fig. 16, two cross sections, CS-I and CS-II, vertical to the heterogeneous surface are defined. L1 and L2 show the corresponding lines of intersection of CS-I and CS-II with the heterogeneous surface respectively.

Fig. 17 and 18 show the evolution of the interface and the corresponding velocity fields on cross section CS-I and CS-II respectively. From Fig. 17, it can be found that the droplet moves to the left. This should be caused by the asymmetry of the wall surface tension with respect to the centre line of the droplet. As shown in Fig. 17, the hydrophilic area occupied by the droplet at the left side of L2 is larger then that at the right side of L2. This means that the wall total surface tension at the

left part of the droplet is larger than right one. Therefore, the droplet tents to reach a steady state when the centre of the droplet reaches a centreline of any strip if the heterogeneous surface is horizontal. See Fig. 18, the cross section connects with the hydrophilic strip of the surface. So, the contact angle is less then 90 degree. Also, the interface and velocity field are symmetric due to the symmetry of the surface tension distribution.
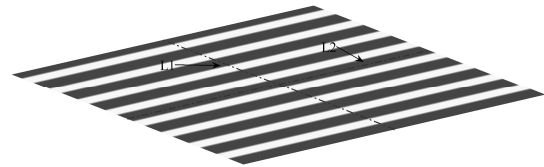

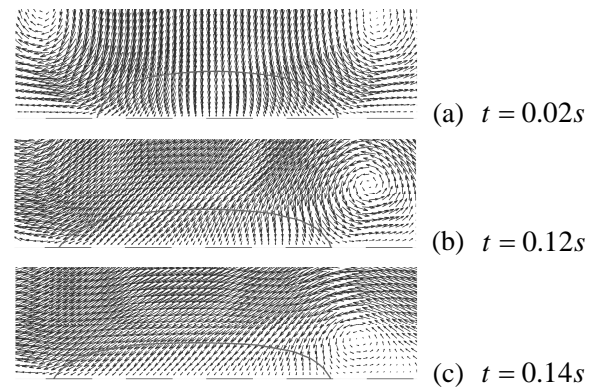Fig. 16: Definition of L1 and L2

(a) $t = 0.02s$

(b) $t = 0.12s$

(c) $t = 0.14s$

Fig. 17: Evolution of interface and the corresponding velocity fields on CS-I.

(a) $t = 0.02s$
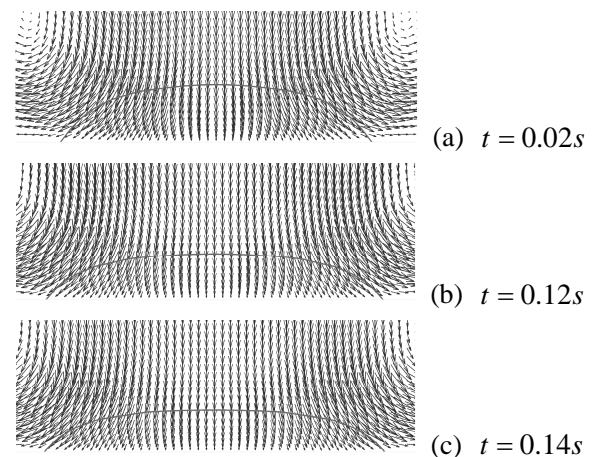
(b) $t = 0.12s$

(c) $t = 0.14s$

Fig. 18: Evolution of the interface and the corresponding velocity fields on CS-II.

7. Conclusions

An overview of the work at Nottingham on developing and applying LBM has been

reported. So far, LBM has been successfully developed or extended to solve fluid dynamic problems including single phase fluid flow and heat transfer on curved and moving boundary, electroosmotically driven flow in thin liquid layer, two-phase flow in mixing layer, viscous fingering phenomena of immiscible fluids displacement, and flow in porous media. In addition, as a major work, a LBM with capability of modelling interaction between two phase fluid and partial wetting surface with relative large density ratio has been reported. Using the method, bubbles/drops flow and coalescence in micro-channels with confined boundary and liquid droplets in gas with large density ratio have been simulated. The results have shown that LBM is a useful tool for mesoscale modelling of single phase and multiphase flow.

8. References

Chen, Shiyi, and Doolen, Gary D., 1998, Lattice Boltzmann method for fluid flows, *Ann. Rev. Fluid Mech.* 30, 329-364.

Chen, W. L., Twu, M. C., and Pan, C., 2002, Gas-liquid two-phase flow in micro-channels, *Int. J. Multiph. Flow*, 28 1235-1247.

Cahn, J. W., 1977. Critical-Point Wetting. J. Chem. Phys. 66**,** 3667-3672.

Dong, B., Yan, Y.Y., Li, W.Z., 2009. Numerical study of the effect of wettability alteration on viscous fingering phenomenon of immiscible fluids displacement in a channel. In: Proceedings of the 17th UK National Conference on Computational Mechanics in Engineering, 69-72.

Gunstensen, A. K., Rothman, D. H., Zaleski, S., and Zanetti, G., 1991, Lattice Boltzmann Model of Immiscible Fluids, *Phys. Rev. A* 43, 4320-4327.

He, X. Y., Chen, S. Y., and Zhang, R. Y., 1999, *J. Comput. Phys.* 152, 642-663.

Inamuro, T., Ogata, T., Tajima, S., and Konishi, N., 2004, *J. Comput. Phys.* 198, 628-644.

Ji, C., Yan, Y.Y., 2008, A molecular dynamics simulation of liquid-vapour-solid system near triple-phase contact line of flow boiling in a microchannel. *Applied Thermal Engineering* 28(2-3), 195-202.

Lee, T., and Lin, C. L., 2005, *J. Comput. Phys.* 206, 16-47.

Martys, N.S., Chen, H., 1996, *Physical Review E*, 53(1), 743.

Mazzitelli, I. M., Lohse, D., and Toschi, F., 2003, The effect of microbubbles on developed turbulence, *Phys. Fluids* 15, L5-L8.

Shan, X.W., and Chen, H. D., 1993, *Phys. Rev. E* 47, 1815-1819.

Succi, S., 2001, *The lattice Boltzmann equation for fluid dynamics and beyond*, Clarendon Press, Oxford.

Swift, M. R., Orlandini, E., Osborn, W. R., and Yeomans, J. M., 1996, Lattice Boltzmann simulations of liquid-gas and binary fluid systems, *Phys. Rev. E*, 54, pp 5041-5052.

Swift, M. R., Osborn, W. R., and Yeomans, J. M., 1995, *Phys. Rev. Lett.* 75, 830-833.

Yan, Y.Y., 2006, Lattice Boltzmann simulation of vortices merging in a two-phase mixing layer. In: *Advanced Computational Methods in Heat Transfer IX*, 87-96.

Yan, Y.Y., et al. 2007. Proceedings of the Institution of Mechanical Engineers, Part C, *J. of Mechanical Engineering Science*, 221(10), 1201-1210.

Yan, Y.Y., Zu, Y.Q., 2007. *J. Computational Physics*, 227 (1), 763-775.

Yan, Y.Y., Zu, Y.Q., 2008a, *Int. J. of Heat and Mass Transfer*, 51(9-10), 2519-2536.

Yan, Y.Y., Zu, Y.Q., 2008b. 6th ASME Conference Darmstadt, ICNMM2008-62162.

Yan, Y.Y., 2009, *Chinese Science Bulletin*, 54(4), 541-548.

Zu, Y.Q., Yan, Y.Y., 2006, Numerical simulation of electroosmotic flow near earthworm Surface, *Journal of Bionic Engineering*, 3, 179-186.